Check for updates

Improved hydrogen uptake of metal modified reduced and exfoliated graphene oxide

Sohan Bir Singh[1], Mahuya De[1,a)]

[1] Department of Chemical Engineering, Indian Institute of Technology Guwahati, Guwahati, Assam 781039, India
a) Address all correspondence to this author. e-mail: mahuya@iitg.ac.in

This study investigated and compared the extent of structural modification and hydrogen uptake of reduced and exfoliated graphene oxides on addition of platinum, nickel and palladium. The addition of all metals affected structure and improved hydrogen uptake but the extent depended on preparation and type of metal. Surface area and pore volume decreased on addition of metals to RGO but increased for EGO. Dense structure of RGO was not affected by platinum, however, changed significantly to fluffy structure on addition of nickel and palladium. The separation of layers increased on addition of palladium to fluffy EGO resulting in its highest surface area and pore volume of 449 m^2/g and 2 cm^3/g, respectively. The highest hydrogen uptake of 3.52 wt% was obtained for Pd/EGO (at – 196 °C, 30 bar) and may be attributed to high surface area, pore volume, O/C ratio and dispersion of palladium particles.

Introduction

Among various carbon-based materials, graphene has extraordinary properties including thermal, mechanical and electrical stabilities [1, 2]. The unique layered structure of graphene results in its significant surface area and pore volume, which are useful for gas storage [2, 3]. The presence of oxygen containing surface functional groups and long range p-conjugation in graphene creates a negatively charged atmosphere suitable for attracting any electropositive adsorbate such as hydrogen. The addition of metals has been reported to further modify the structure as well as adsorption capacity of graphene-based materials. The graphene layers dispersed with different transition metals including Pt, Ni, Pd, Ti and Fe have been reported [3–7]. The presence of metals on graphene is reported to enhance the interactions between molecular hydrogen and graphene surface [4, 7, 8].

The structure of reduced graphene oxide (RGO) was reported to change from coagulated wavy shape to more compact wavy shape on doping of 10 wt% Pd, while horizontal aligned shape was observed on doping of 10 wt% Ni [6]. The same group reported that corresponding hydrogen uptake capacity increased from 2 to 2.8 and 2.7 wt%, respectively, on addition of Pd and Ni, at – 196 °C and 20 bar [6]. Hong et al. [3] reported that the thickness of single layer graphene oxide (GO) to be around 1.0 nm and enhanced up to 2.1 nm with addition of V_2O_5 and TiO_2. The morphology appeared like GO sheet wrapped uniformly on the V_2O_5 and TiO_2. A positive enhancement in hydrogen uptake of GO was also reported with the addition of V_2O_5 and TiO_2. The hydrogen uptake capacities were 1.26 and 1.36 wt% for TiO_2 and V_2O_5-doped graphene oxide (GO), respectively at – 196 °C and 60 bar. This increase was assigned to metal oxides that provided additional active sites and interspace between GO wrapped metal oxide composite structure. However, no effects on the crumpled paper structure as well as hydrogen adsorption capacity of exfoliated graphene oxide were noticed by Huang et al. [4] on incorporation of Pt and Pd. From density functional theory calculation, Bhattacharya and coworkers [9] reported that the transition metal atoms adsorbed around the defect sites of graphene showed stronger bonding interaction with the graphene lattice. This interaction led to well dispersion of the metal particles and enhanced the hydrogen uptake of graphene. Huston et al. [10] reported that with addition of iron to exfoliated graphene oxide, the surface area was reduced from 375 to 190 m^2/g but the hydrogen uptake was slightly enhanced from 2.07 to 2.16 wt% at – 196 °C and 50 bar. The hydrogen uptake capacity of different metal modified graphene at – 196 °C are summarized in Supplementary Table S1.

The authors came across limited studies on the effect of presence of metals on structural changes of graphene prepared by different methods and subsequent effects on hydrogen uptake. In the present study, three metals Pt, Ni or Pd were selected for

deposition on graphene layers. The effect of addition of metals on their structural properties and subsequently on their hydrogen adsorption capacities was investigated and compared. These three metals were selected based on their reported activity in hydrogenation and dehydrogenation reactions. Both reduced graphene oxide (RGO) and exfoliated graphene oxide (EGO) were used as base graphene materials. The hydrogen storage properties were determined at − 196 °C and a moderate pressure of 30 bar using volumetric apparatus.

Results and discussion

The elemental composition of the samples was determined by EDX and summarized in Table 1. The EDX spectra of the samples are shown in Supplementary Fig. S1. The final average loading of metals was about 2 wt% for all the samples. RGO showed oxygen content of 10.4 wt% with oxygen–carbon ratio (O/C) of 0.12. The EGO showed oxygen content of 20.9 wt% corresponding to O/C ratio of 0.26. This suggested that during exfoliation in presence of air, higher number of oxygen containing functional groups were retained between graphene surfaces. When RGO was doped with metals, the oxygen content was observed to be slightly higher for metal-doped samples. The highest oxygen content of 13.0 wt% was obtained for the Pd/RGO sample. Accordingly, with addition of metals, oxygen–carbon ratio (O/C) increased in the order of 0.12 (RGO) < 0.13 (Ni/RGO) < 0.14 (Pt/RGO) < 0.15 (Pd/RGO). Metals are reported to interact with oxygen on coming in contact with the same [11, 12]. The deposited metals may have interacted with the surface oxygen present in their vicinity and helped in its retainment, highest being for Pd/RGO sample. The higher oxidation potential for palladium metal may have resulted in more interaction of palladium with surface oxygen, resulting in their more retainment for Pd/RGO sample.

In contrast to Pd/RGO, with addition of Pd the oxygen content was reduced for Pd/EGO to 18.6 wt% from 20.9 wt% for EGO. The corresponding O/C ratios were reduced to 0.23 from 0.26 for EGO. Here, the decrease in oxygen content for palladium-doped sample might have resulted from the

involvement of some surface oxygens in partial combustion of carbon matrix during exfoliation. The presence of metal has catalytic effect and lowers the combustion temperature of carbon matrix [13].

The XRD profiles of different metal-doped RGO samples are compared in Fig. 1a. The RGO displayed peak at $2\theta = 24.5°$ due to presence of C(002) graphitic zone [14]. For all the metal-doped RGO samples, the peak due to the metal was observed in addition to the graphitic peak at $2\theta = 24.5°$. For Ni/RGO, the low intensity peak at $2\theta = 44.4°$ may be attributed to (111) plane of metallic nickel Ni° [15]. For Pt/RGO, the three peaks at $2\theta = 39.85°$, 46.3° and 67.1° corresponded to Pt° (111), Pt° (200) and Pt° (220) planes, respectively [4, 16]. In the case of Pd/RGO, the peaks at $2\theta = 39.9°$, 46.6° and 67.85° resulted from the planes of Pd° (111), Pd° (200) and Pd° (220), respectively [17, 18]. The XRD peaks confirmed that the metals were mostly present in zero oxidation state or metallic state in the samples. This agreed with the reducing conditions prevailed during their preparation due to presence of hydrazine. The comparison of the graphitic peaks of the samples (supplementary Fig. S2) showed that the addition of Pd or Ni slightly increased the graphitic zone in doped samples, while for Pt the effect was insignificant. The increase in intensity of graphitic peak on addition of palladium and nickel to graphene was also observed by Ismail et al. [6]. For EGO sample, mainly the graphitic peak at $2\theta = 24.5°$ was observed. The addition of Pd to EGO, also increased the graphitic zone significantly. This increase may be accounted by catalytic effect of metal on the formation of graphitic zone during exfoliation at high temperature of 300 °C. Three XRD peaks attributed to Pd° were observed at $2\theta = 39.9°$, 46.6° and 67.85° in Pd/EGO sample similar to that observed for Pd/RGO. No peaks for metal oxide form was observed to be present in the sample. The d-spacing values determined from XRD profiles, are tabulated in Table 2. The RGO had *d*-spacing of 0.39 nm. The *d*-spacing decreased on the doping of different metals. For doped RGO samples the *d*-spacing was about 0.36 nm. For EGO, the *d*-spacing was 0.38 and decreased to 0.34 nm for Pd/EGO. This decrease in separation between the layers for all the doped samples may be attributed to deposited metal particles in between the layers of the graphene.

The Raman spectra of the samples are shown in Fig. 1b. The D band was detected in range of 1346–1350 cm^{-1} and G band around 1591–1597 cm^{-1}. The intensity ratios (I_D/I_G) of the samples, shown in Fig. 1b, were calculated using height of D and G bands. With the incorporation of metals to RGO, the value of I_D/I_G increased from 0.89 for RGO to 1.08, 1.10 and 1.26, for nickel, palladium and platinum-doped RGO samples, respectively. The EGO samples had intensity ratio (I_D/I_G) of 0.90, which on palladium doping increased to 1.05. Incorporation of metals increased the defects on the graphene surface, thereby increasing the (I_D/I_G) ratio in metal modified samples [7].

TABLE 1: Elemental analysis of samples using EDX.

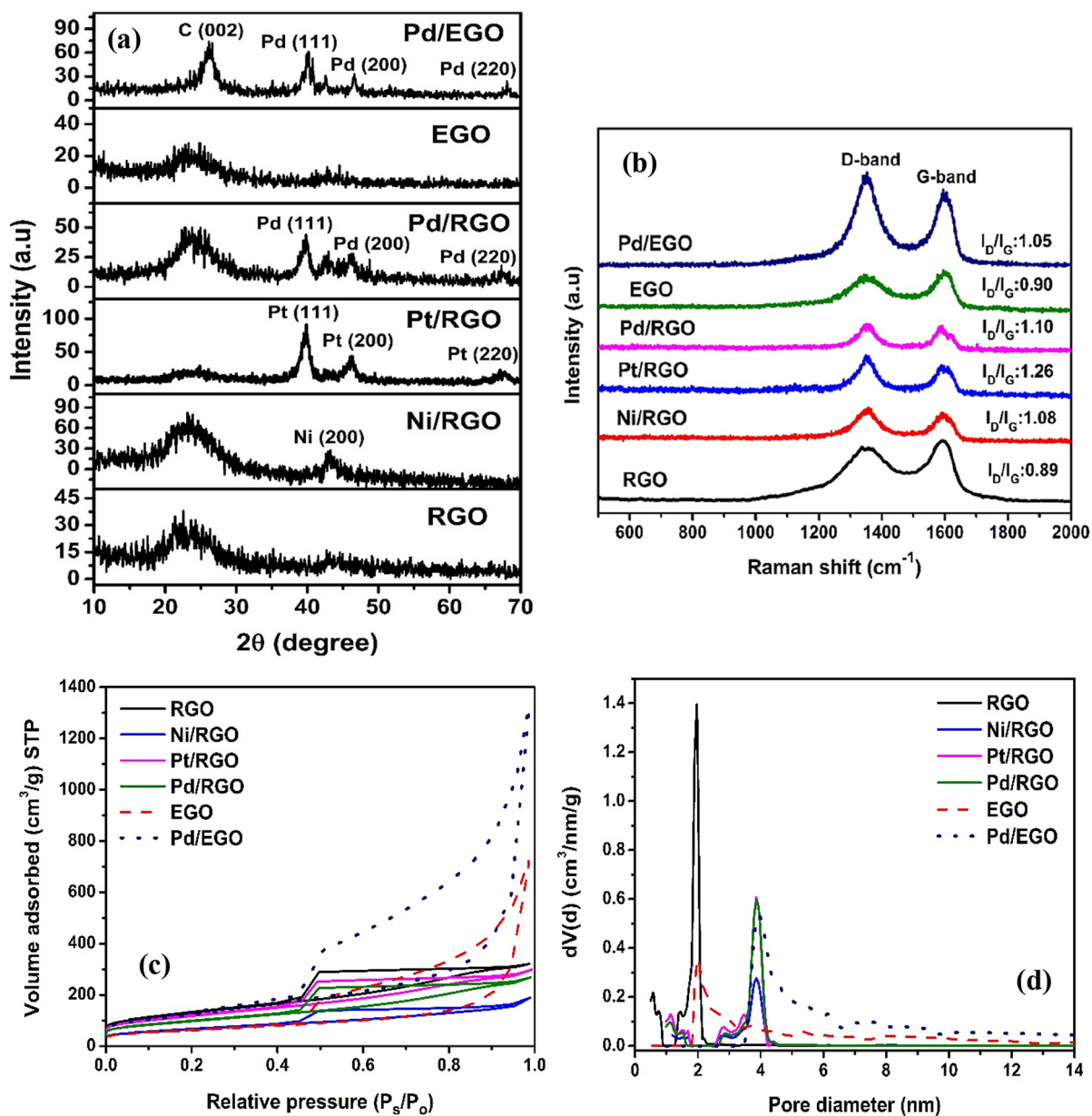| Sample ID	EDX elements (wt%)			
	Metals	C	O	O/C
RGO	–	89.6	10.4	0.12
Ni/RGO	2.2	86.3	11.5	0.13
Pt/RGO	2.0	86.1	11.9	0.14
Pd/RGO	2.3	84.7	13.0	0.15
EGO	–	79.1	20.9	0.26
Pd/EGO	2.0	79.4	18.6	0.23

Figure 1: (a) XRD profiles (b) Raman spectra with intensity ratios (I_D/I_G) calculated from D and G bands height (c) N$_2$ adsorption–desorption isotherms (d) Pore size distribution of samples.

The nitrogen adsorption–desorption isotherms (Fig. 1c) of all the RGO-based samples were type-II with wide H4-type hysteresis loop, signifying slit-shaped pores. As can be observed, the impregnation of metal did not affect the overall pore structure. However, the volume of nitrogen adsorption significantly decreased. This decrease may be associated with blockage of openings between the layers due to the presence of the metal clusters. The most significant decrease in volume adsorbed was observed for the nickel-doped RGO sample. Accordingly, the lowest surface area and pore volume were observed for Ni/RGO sample (Table 3). However, the nature of isotherm differed for

EGO samples and type IV with H4-type hysteresis loop was observed. No change in nature of isotherm or hysteresis loop was observed when palladium was doped on EGO sample. The very wide hysteresis loop was clearly observed for both EGO and Pd/EGO samples at a higher relative pressure (P_s/P_o) of above 0.4. This suggested presence of higher amount of mesopores in these samples as compared to that in RGO-based samples. Also, the volume of nitrogen adsorbed was significantly higher for EGO-based samples.

The BET surface area and total pore volume of all the metal-doped RGO samples reduced compared to that of RGO (461

TABLE 2: Lattice spacing, number of layers and average particle size of the samples.

Sample ID	XRD	AFM		TEM	
	d-spacing (nm)(002)	Average thickness (nm)	Number of layers	Average metal particle size (nm)	Metal dispersion (%)
RGO	0.39	7.32	18	–	–
Ni/RGO	0.35	7.08	17	3.8	29
Pt/RGO	0.36	6.14	15	3.4	33
Pd/RGO	0.35	5.96	14	2.6	43
EGO	0.38	6.23	15	–	–
Pd/EGO	0.34	3.12	7	2.5	45

TABLE 3: Surface area and pore analysis of the samples.

Sample ID	BET surface area (m²/g)	Total pore volume (cm³/g)	Micropore area (m²/g)	Average pore size (nm)
RGO	461	0.50	86	1.80
Ni/RGO	234	0.29	16	3.88
Pt/RGO	417	0.46	39	3.87
Pd/RGO	345	0.41	40	3.83
EGO	227	1.20	15	2.81
Pd/EGO	449	2.04	4	4.78

m^2/g, 0.50 cm^3/g). This decrease may have happened from blockage of the open spaces in RGO by the metal particles as mentioned earlier. Micropore pore area of 86 m^2/g was observed for RGO. With addition of metals to RGO, micropore pore area was also reduced. The most significant drop in area was observed for nickel-doped RGO sample. However, on metal doping the surface area and pore volume almost doubled for Pd/EGO sample compared to that of EGO. This significant enhancement may be attributed to better separation of layers during exfoliation in presence of metal. As stated earlier for preparation of metal-doped EGO, the metal was added to GO and the metal–GO composite was subjected to exfoliation temperature of 300 °C. The metal had a significant catalytic effect in the combustion of carbon [14]. This may have facilitated combustion at lower temperature and thereby, better separation of layers by generated gases. Similar observation was also reported by Li et al. [19]. Negligible micropore area was observed for EGO-based samples.

The pore size distributions of the samples are shown in Fig. 1d. The RGO seemed to have pores in very narrow range between 0.4 to 2.2 nm, showing mainly microporous nature. When impregnated with different metals, the pore distribution was shifted toward the larger pores. Pores were observed mainly in the mesoporous range of 2.6 to 4.4 nm for all the metal-doped RGO samples, with the average pore size of 3.8 nm.

In contrast for the EGO sample, pores were observed mainly in the mesoporous region of 2–5 nm. Addition of metals further shifted the pore size distribution to higher value. The average pore size of 2.81 nm for EGO shifted to 4.78 nm for Pd/EGO. For all the doped samples shifting of average pore size to higher values suggested partial blockage of smaller pores in presence of metal clusters.

The AFM topography images and corresponding height profiles of the samples are shown in Fig. 2. The number of layers was evaluated from their average thickness of layers and reported theoretical thickness of 0.40 nm for single graphene layer [20, 21]. The average thickness and corresponding number of layers of the samples are included in Table 2. The average thickness was obtained between 3.12 and 7.32 nm, while number of layers were in the range of 7–18. It was observed that the average thickness and number of layers were reduced when metals were doped on both RGO and EGO samples. This suggested metals to be effective for layer separation. The most effective layer separation was noticed for Pd-doped EGO sample, and number of layers were reduced from 15 to 7.

The presence of oxygen containing functional groups and oxidation state of Pd in samples were characterized using XPS analysis. The C1s and Pd 3d spectra of the samples are shown in Fig. 3. The C1s spectra showed three peaks at 284.8, 286.2 and 287.8 eV in all the samples, which corresponded to C–C (sp^2 bonds), C–O (epoxy) and C=O (carbonyl) functional groups, respectively [22, 23]. This suggested presence of oxygen containing functional groups. The presence of oxygen containing functional groups was also confirmed by O1s peaks and the spectra are shown in Supplementary Fig. S3. The O1s peaks were observed at 531.5, 533.5 and 537.7 eV, which may be assigned to C=O (carbonyl group), C–O (epoxy group) and C–OH (hydroxyl group), respectively [23, 24]. Figure 3e, f showed the presence of Pd in two chemical states of $3d_{3/2}$ and $3d_{5/2}$ [25]. The peaks found with lower binding energies at 335.6 and 340.8 eV corresponded to the Pd^0 state, while peaks with higher binding energies observed at 337 and 342.1 eV may be assigned to Pd^{2+} state [26]. The relative surface concentration in percentage of Pd^0/Pd^{2+} ratios were 80/20 and 75/25 for Pd/RGO and Pd/EGO, respectively. The Pd mainly existed in metallic form in both the samples. The predominance of metallic state was also reflected in the results of XRD. The O/C ratios determined from the XPS analysis (Supplementary Table S3) agreed with the values obtained from EDX analysis.

The FESEM images of RGO and doped RGO samples are shown in Fig. 4. Presence of dense layers with very fine pores was observed for the RGO sample. Morphology significantly changed with the incorporation of metals into RGO and depended on the type of metal. Fluffy and layers structures appeared for nickel and palladium-doped RGO. The palladium-doped RGO had more uniform structure compared to that
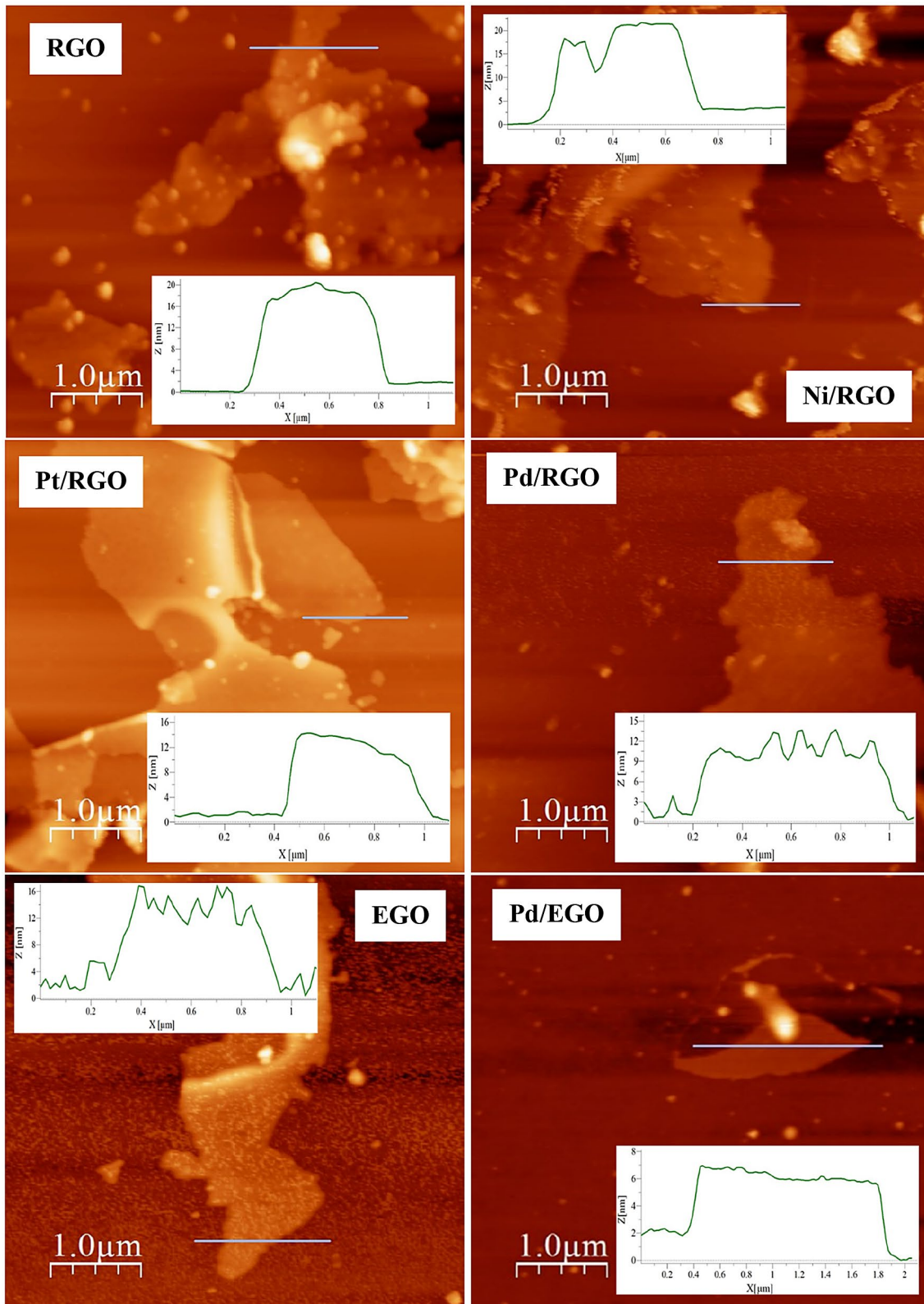
Figure 2: AFM topography images with corresponding height profiles of samples.
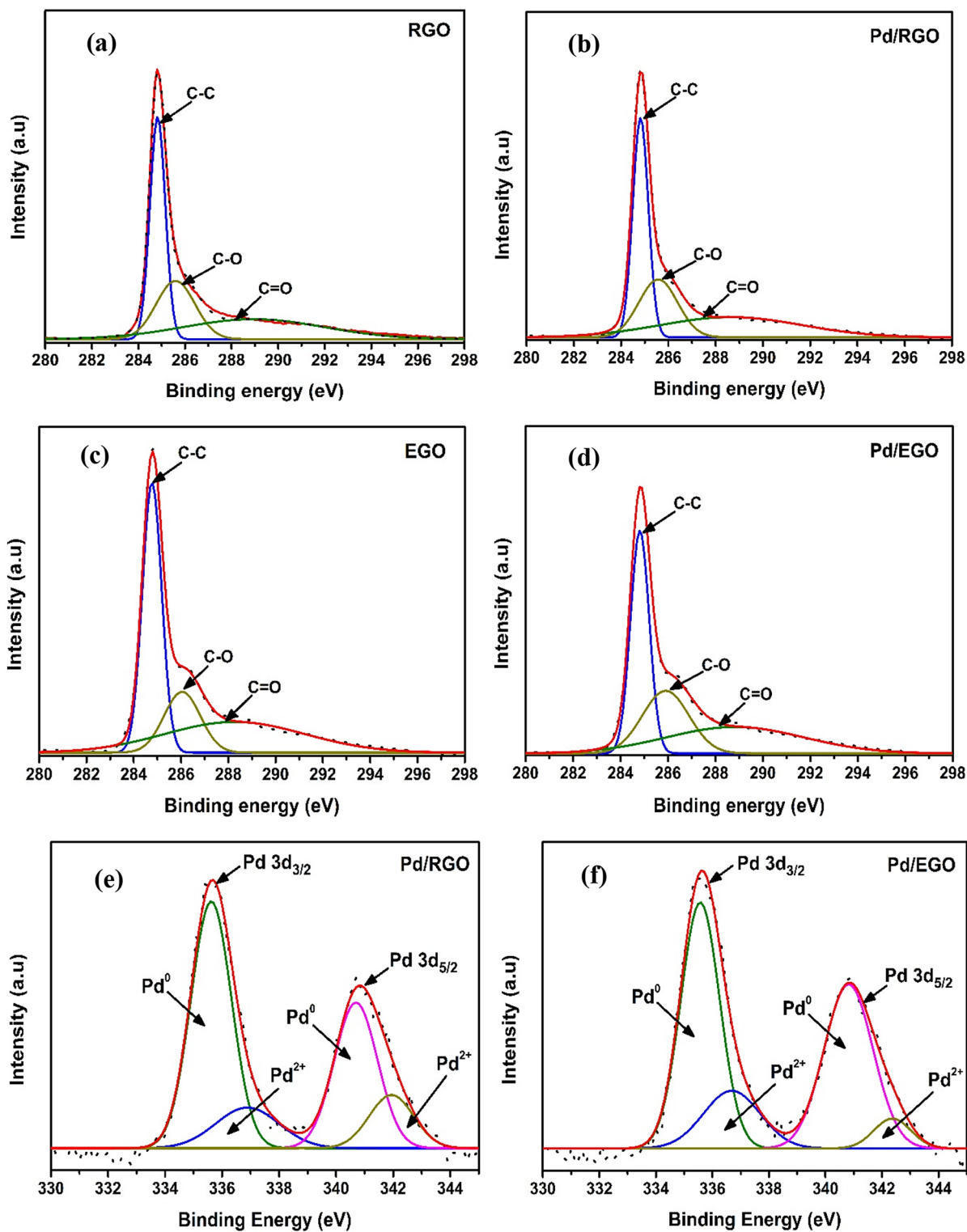
Figure 3: C1s XPS spectra of (a) RGO (b) Pd/RGO (c) EGO (d) Pd/EGO and Pd 3d spectra of (e) Pd/RGO (f) Pd/EGO.

of nickel-doped RGO. The nickel-doped RGO showed non-homogenous and less separated layers with large blank spaces in between. This may be the reason for the comparatively low surface area and pore volume of Ni/RGO as observed earlier.

The platinum-doped RGO showed almost similar structure as that of undoped RGO, only bit more dense. This resulted in least effect on surface area and pore volume of RGO and gave highest values among doped RGO samples (Table 3). The FESEM
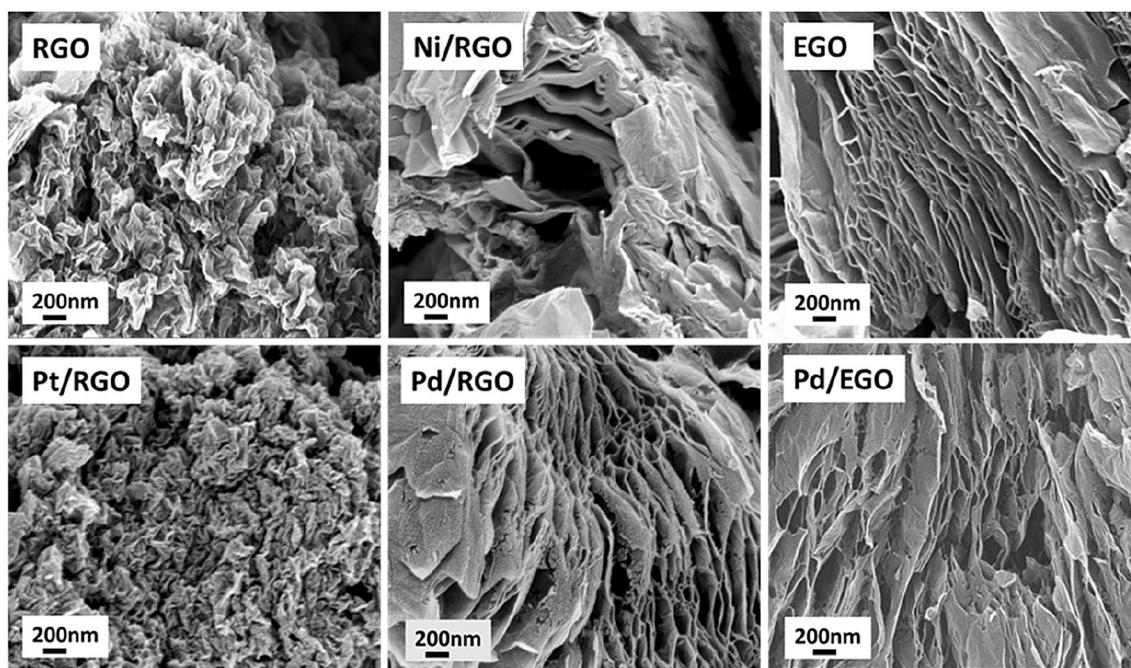
Figure 4: FESEM images of samples.

images of EGO showed fluffy homogeneous layered structure. With addition of metal the separation of layers increased for Pd/EGO and may be the reason for the significant increase in surface area and pore volume of this sample.

TEM images of the samples are shown in Fig. 5a. The corresponding metal size distribution is shown in Fig. 5b. The well and uniform distribution of metal particles on or inside the layers were observed from TEM images. This was also observed by EDX mapping of metal-doped samples (Supplementary Fig. S4). The TEM structure of the samples agreed with FESEM analysis. The metal dispersion in percentage was evaluated by the Eq. 1 using average metal particles size obtained from TEM analysis: [27]

$$\text{Metal dispersion (\%)} = \frac{1.13}{\text{average metal particles size (nm)}} \times 100$$

(1)

All the metal particles were assumed to have spherical shape. The metal dispersion and metal average size are included in Table 2. The average sizes of metals were obtained as 2.6 nm for Pd/RGO, 3.4 nm for Pt/RGO and 3.8 nm for Ni/RGO. The corresponding dispersion values of Ni, Pt and Pd, were 29, 33 and 43%, respectively. Thus, the palladium metal particles showed higher dispersion compared to that of nickel and platinum. The Pd/EGO had the lowest average size of Pd particles at 2.5 nm and corresponding Pd dispersion of 45% was highest. The higher dispersion of palladium metal suggested higher interaction between palladium metal and carbon matrix. Lower interaction between platinum and RGO was also confirmed from the

FESEM images as the RGO structure was least affected by the presence of platinum. Less reduction in surface area and pore volume for Pt/RGO compared to RGO also agreed with this observation. Similar behavior of platinum was also observed by Baca et al. [28]. The higher size for nickel cluster agreed with its sintering tendency resulting in lowest surface area and pore volume for Ni/RGO sample.

Hydrogen uptake

Hydrogen adsorption isotherms of all the samples are shown in Fig. 6a and the hydrogen uptake values at − 196 °C and 30 bar are included in Fig. 6b. The RGO sample had hydrogen uptake capacity of 2.50 wt%. With the addition of metals in RGO, a positive effect on hydrogen uptake was observed for all the samples. The uptake capacity order was 2.50 (RGO) < 2.64 (Ni/RGO) < 2.8 (Pt/RGO) < 3.22 (Pd/RGO) wt%. It can be observed that all the doped RGO samples showed higher hydrogen uptake in spite of lower surface area and pore volume for the doped sample. The anomaly can be explained based on presence of metal. The metal sites provided the additional and stronger sites for interaction with the incoming hydrogen molecule. Hence, at higher metal dispersion the available active sites for hydrogen uptake were higher, at same metal loading. With addition of metals some of the adsorption sites were lost due to decrease in surface area. However, this was compensated by increase in relatively stronger metal-based adsorption sites. The hydrogen is also reported to interact more strongly with palladium
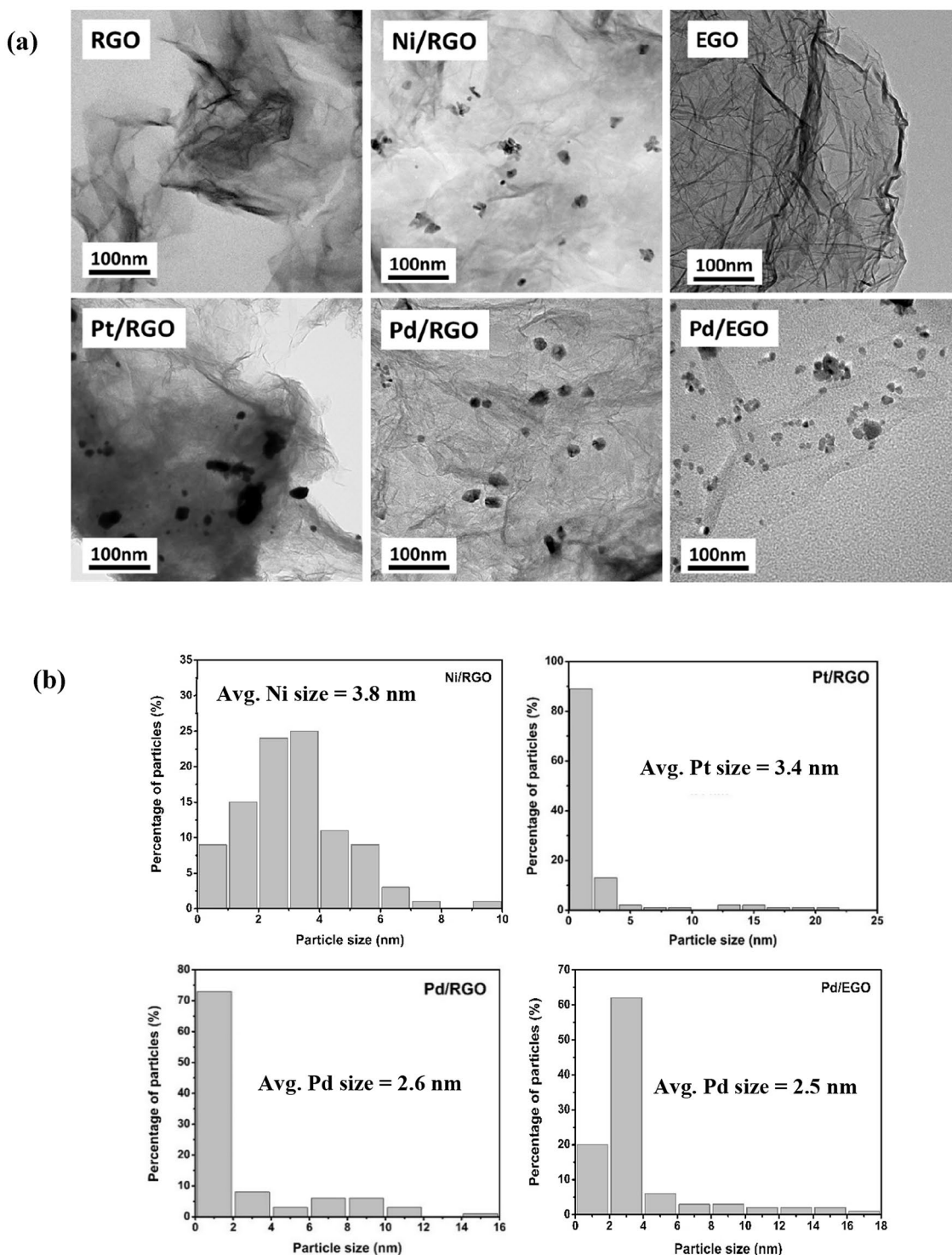
Figure 5: (a) TEM images (b) particle size distribution of doped samples.

compared to that with nickel and platinum [28, 29]. Among doped RGO samples, the highest hydrogen uptake of 3.22 wt% for Pd/RGO may have resulted from highest dispersion and strongest interaction of palladium particles with hydrogen.

EGO sample showed higher hydrogen uptake capacity than all the RGO samples in spite of lower surface area. These higher uptake values might be explained by the combined effect of fluffy layered structure and higher pore volume. The presence of oxygen containing surface functional groups may have also
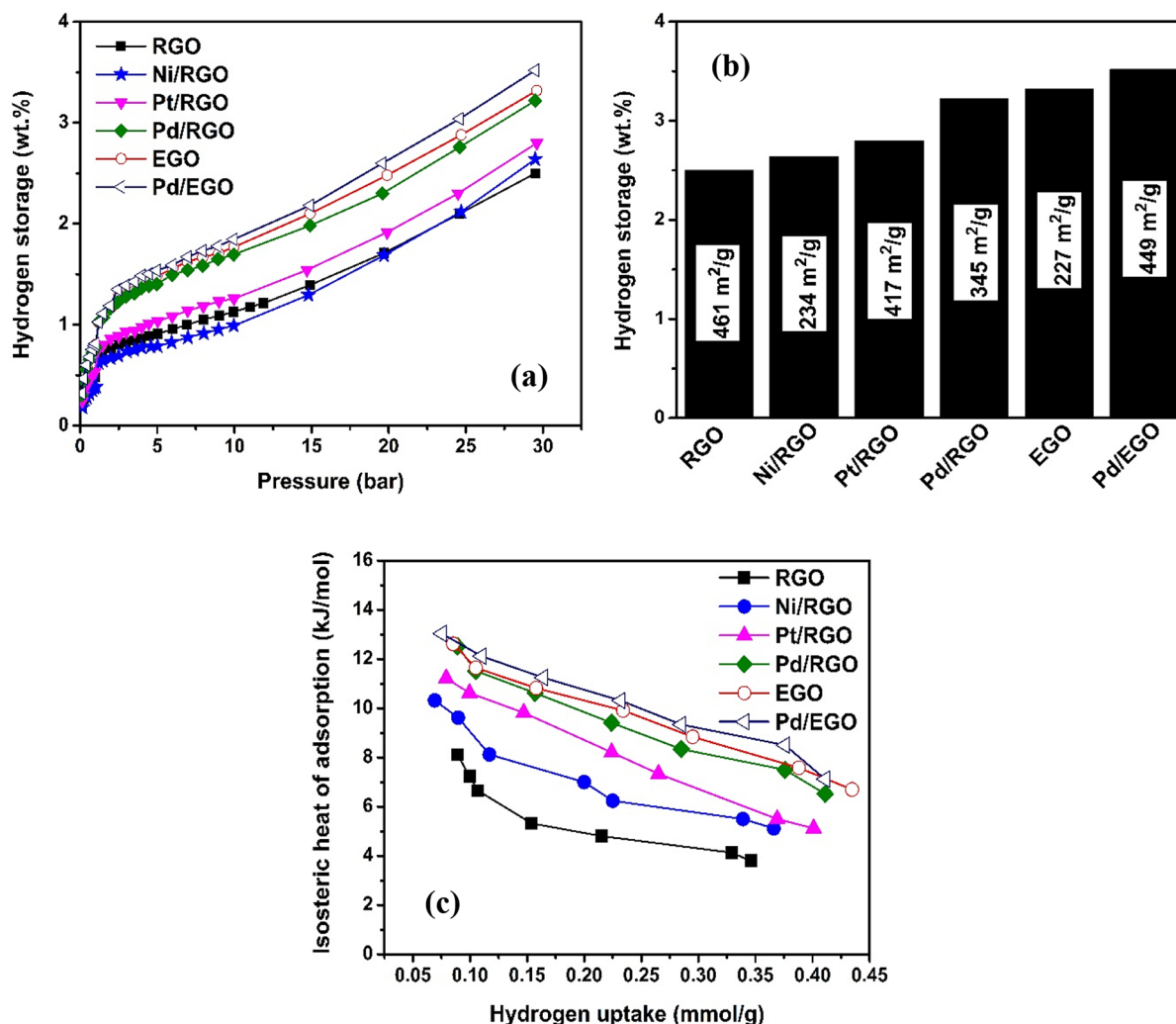
Figure 6: (a) Hydrogen adsorption isotherms at −196 °C up to 30 bar. (b) Hydrogen storage at −196 °C and 30 bar of the samples. (c) Isosteric heats of adsorption as a function of the amount of H$_2$ adsorbed on samples.

positively contributed to hydrogen uptake of EGO samples. The presence of surface oxygen rendered more electronegative character to the surface, thereby facilitating its interaction with the highly electropositive hydrogen. Addition of palladium to EGO further increased the hydrogen uptake and the Pd/EGO showed the highest hydrogen uptake of 3.52 wt%. The higher surface area of this sample than EGO and presence of highly interactive metal sites might have contributed to its highest hydrogen uptake.

The isosteric heat of adsorption (Q_{ads}) was calculated from the adsorption isotherms. The variation in calculated isosteric heat of adsorption with hydrogen uptake is shown in Fig. 6c. The isosteric heat of adsorption for RGO was 8 kJ/mol at lower hydrogen uptake, which was enhanced to the range 10–13 kJ/mol on doping of different metals. The increasing order of heat of adsorption for doped RGO (in kJ/mol) was Ni/RGO (10) < Pt/RGO (11) < Pd/RGO (13). The higher heat of adsorption for

metal-doped samples indicated a significant interaction between hydrogen and metal particles. At higher hydrogen uptake, the heat of adsorption was exhibited between 5–7 kJ/mol, with highest value being for the Pd/RGO sample (7 kJ/mol). The heat of adsorption on Pd/EGO sample (13 kJ/mol) was highest indicating strongest interaction between hydrogen and highly dispersed palladium particles. These values agreed with the reported heat of adsorption values for RGO (3–6 kJ/mol) and metal (Pt & Pd)-doped graphene (8–17 kJ/mol) [2].

Conclusion

This study investigated and compared the extent of modification on structure and hydrogen adsorption capacity of reduced and exfoliated graphene oxides on addition of platinum, nickel and palladium. The addition of all metals affected the structure and improved hydrogen uptake but the extent depended

on preparation and type of metal. The decrease in d-spacing was observed on addition of metals to both RGO and EGO. This decrease may be attributed to deposited metal particles in between the layers. The RGO (461 m^2/g) showed microporous nature with an average pore size of 1.8 nm. With addition of different metals, the pore distributions were shifted toward mesopores with average pore size in the range of 3.8–3.9 nm for doped RGO. The surface area and total pore volume of all metal-doped RGO samples were reduced compared to that of RGO. However, the effect was reverse when palladium was added to EGO sample. The surface area (227 m^2/g) and pore volume (1.2 cm^3/g) of EGO increased to almost double values of 449 m^2/g and 2.04 cm^3/g, respectively for Pd/EGO. The highest dispersion of metal was observed for Pd/RGO. The RGO showed dense layered structure with very fine pores. The morphology of RGO was not affected significantly with addition of platinum. However, addition of nickel and palladium changed the structure of RGO to fluffy and layered structures. For EGO, which already had fluffy structures, the separation of layers further increased on addition of palladium. This resulted in its highest surface area and pore volume. The highest hydrogen uptake of 3.52 wt% was obtained for Pd/EGO at – 196 °C and 30 bar. The highest uptake may be attributed to the highest surface area, pore volume, O/C ratio and dispersion of palladium particles in of Pd/EGO. The Pd /RGO gave the second highest hydrogen uptake of 3.22 wt% among doped samples. This was in spite of having the lower surface area and pore volume than the Pt/RGO. The higher hydrogen uptake capacity of Pd/RGO may have resulted from higher dispersion of metal particles, higher oxygen content and layered structure. Also, higher interaction of Pd and hydrogen might have contributed to higher hydrogen uptake of Pd containing samples. The heat of adsorption was also highest for Pd/EGO sample (13 kJ/mol), confirming strongest interaction between hydrogen and highly dispersed palladium particles.

Experimental

Preparation

The graphene oxide (GO) was first prepared by modified Hummer's method [30]. The desired metal (Ni, Pt or Pd) was impregnated on the graphene oxide (GO). The dry metal-doped GO sample was divided into two parts. One part was reduced by hydrazine to obtain the metal-doped RGO and the remaining part was exfoliated to obtain the metal-doped EGO sample. The details of the preparation steps are shown in Fig. S5. The required amount of metal (Pt/Ni/Pd) precursor was dissolved in deionized water and aqueous solution was added drop wise to GO. The chloroplatinic acid hexahydrate (Sigma-Aldrich, $H_2Cl_6Pt\cdot6H_2O$, 37.5%), palladium chloride (Sigma-Aldrich, Pd Cl_2, 99%) and nickel acetate tetrahydrate (Sigma-Aldrich, $Ni(OCOCH_3)_2\cdot4H_2O$, 98%) were used as precursors for the

metals. The resultant metal–GO mixture was thoroughly mixed to form a homogeneous sample. This wet metal–GO composite sample was dried at 60 °C for 12 h. The dry metal–GO composite was divided into two parts. For the preparation of metal-doped reduce graphene oxide (M/RGO), about 1 g of the dry metal–GO composite sample was dispersed in 300 ml of deionized water. The suspension of metal–GO composite was stirred and then sonicated at room temperature for 2 h followed by addition of hydrazine at 90 °C and treated for 6 h. The final sample after drying gave metal-doped RGO denoted as Pt/RGO, Ni/RGO or Pd/RGO.

The metal-doped exfoliated graphene oxide (M/EGO) was prepared using palladium as metal precursor. Around 1 g of dried palladium–GO composite sample was taken into a quartz boat and placed in the horizontal furnace. The temperature of the furnace was increased from room temperature to 300 °C under air flow. The sample was maintained at an exfoliation temperature of 300 °C for 1 h in the same flow of air. Thereafter, the furnace was cooled down to room temperature. The obtained sample was palladium-doped EGO and named as Pd/EGO.

For preparation of RGO and EGO samples, the same steps of hydrazine reduction and air exfoliation were carried out respectively, as described for doped samples. However, in this case, directly GO was used as the base material instead of metal–GO composite.

Characterization of materials

The metal-doped RGO and EGO samples were characterized by various analytical techniques, such as X-ray diffraction (XRD), X-ray photoelectron spectroscopy (XPS), Raman spectroscopy, surface area and pore volume analysis, field emission scanning electron microscopy (FESEM), energy dispersive X-ray (EDX) and transmission electron microscopy (TEM). The details of the characterization are added in Supplementary Table S2. Hydrogen adsorption analysis was performed at different temperatures up to pressure of 30 bar by volumetric method. The more details are incorporated in Supplementary Table S2.

Acknowledgments

Declarations

Conflict of interest On behalf of all authors, the corresponding author states that there is no conflict of interest.

Supplementary Information

The online version contains supplementary material available at https://doi.org/10.1557/s43578-021-00331-1.

References

1. N. Bader, A. Ouederni, Optimization of biomass-based carbon materials for hydrogen storage. J Energy Storage **5**, 77 (2016)

2. S. Gadipelli, Z.X. Guo, Graphene-based materials: Synthesis and gas sorption, storage and separation. Prog. Mater. Sci **69**, 1 (2015)

3. W.G. Hong, B.H. Kim, S.M. Lee, H.Y. Yu, Y.J. Yun, Y. Jun, J.B. Lee, H.J. Kim, Agent-free synthesis of graphene oxide/transition metal oxide composites and its application for hydrogen storage. Int. J. Hydrogen Energy **37**, 7594 (2012)

4. C.-C. Huang, N.-W. Pu, C.-A. Wang, J.-C. Huang, Y. Sung, M.-D. Ger, Hydrogen storage in graphene decorated with Pd and Pt nano-particles using an electroless deposition technique. Separ. Purif. Technol. **82**, 21 (2011)

5. J.A. Alonso, I. Cabria, M.J. López, Simulation of hydrogen storage in porous carbons. J. Mater. Res. **28**, 589 (2013)

6. N. Ismail, M. Madian, M.S. El-Shall, Reduced graphene oxide doped with Ni/Pd nanoparticles for hydrogen storage application. Ind. Eng. Chem. Res **30**, 328 (2015)

7. V.B. Parambhath, R. Nagar, S. Ramaprabhu, Effect of nitrogen doping on hydrogen storage capacity of palladium decorated graphene. Langmuir **28**, 7826 (2012)

8. A. Klechikov, J. Sun, G. Hu, M. Zheng, T. Wågberg, A.V. Talyzin, Graphene decorated with metal nanoparticles: hydrogen sorption and related artefacts. Microporous Mesoporous Mater. **250**, 27 (2017)

9. A. Bhattacharya, S. Bhattacharya, C. Majumder, G. Das, Transition-metal decoration enhanced room-temperature hydrogen storage in a defect-modulated graphene sheet. J. Phys. Chem. C **114**, 10297 (2010)

10. M.S.L. Hudson, H. Raghubanshi, S. Awasthi, T. Sadhasivam, A. Bhatnager, S. Simizu, S. Sankar, O. Srivastava, Hydrogen uptake of reduced graphene oxide and graphene sheets decorated with Fe nanoclusters. Int. J. Hydrogen Energy **39**, 8311 (2014)

11. S. Shaikhutdinov, M. Heemeier, J. Hoffmann, I. Meusel, B. Richter, M. Baumer, H. Kuhlenbeck, J. Libuda, H.-J. Freund, R. Oldman, S.D. Jackson, C. Konvicka, M. Schmid, P. Varga, Interaction of oxygen with palladium deposited on a thin alumina film. Surf. Sci. **501**, 270 (2002)

12. T. Li, P.B. Balbuena, Computational studies of the interactions of oxygen with platinum clusters. J. Phys. Chem. B **105**, 9943 (2001)

13. S.B. Singh, M. De, Scope of doped mesoporous (< 10 nm) surfactant-modified alumina templated carbons for hydrogen storage applications. Int. J. Energy Res. **43**, 4264 (2019)

14. Y. Wang, C.X. Guo, X. Wang, C. Guan, H. Yang, K. Wang, C.M. Li, Hydrogen storage in a Ni–B nanoalloy-doped three-dimensional graphene material. Energy Environ. Sci. **4**, 195 (2011)

15. A. Yadav, M. Faisal, A. Subramaniam, N. Verma, Nickel nanoparticle-doped and steam-modified multiscale structure of carbon micro-nanofibers for hydrogen storage: effects of metal, surface texture and operating conditions. Int. J. Hydrogen Energy **42**, 6104 (2017)

16. H. Oh, T. Gennett, P. Atanassov, M. Kurttepeli, S. Bals, K.E. Hurst, M. Hirscher, Hydrogen adsorption properties of platinum decorated hierarchically structured templated carbons. Microporous Mesoporous Mater. **177**, 66 (2013)

17. D. Giasafaki, A. Bourlinos, G. Charalambopoulou, A. Stubos, T. Steriotis, Synthesis and characterisation of nanoporous carbon–metal composites for hydrogen storage. Microporous Mesoporous Mater. **154**, 74 (2012)

18. V.B. Parambhath, R. Nagar, K. Sethupathi, S. Ramaprabhu, Investigation of spillover mechanism in palladium decorated hydrogen exfoliated functionalized graphene. J. Phys. Chem. C **115**, 15679 (2011)

19. Z. Li, Z. Zhou, G. Yun, K. Shi, X. Lv, B. Yang, High-performance solid-state supercapacitors based on graphene-ZnO hybrid nanocomposites. Nanoscale Res. Lett. **8**, 1 (2013)

20. N.-W. Pu, C.-A. Wang, Y. Sung, Y.-M. Liu, M.-D. Ger, Production of few-layer graphene by supercritical CO2 exfoliation of graphite. Mater. Lett. **63**, 1987 (2009)

21. S. Stankovich, D.A. Dikin, G.H. Dommett, K.M. Kohlhaas, E.J. Zimney, E.A. Stach, R.D. Piner, S.T. Nguyen, R.S. Ruoff, Graphene-based composite materials. Nature **442**, 282 (2006)

22. I.R. Kottegoda, X. Gao, L.D. Nayanajith, C.H. Manorathne, J. Wang, J.-Z. Wang, H.-K. Liu, Y. Gofer, Comparison of few-layer graphene prepared from natural graphite through fast synthesis approach. J. Mater. Sci. Technol. **31**, 907 (2015)

23. Y.-E. Shin, Y.J. Sa, S. Park, J. Lee, K.-H. Shin, S.H. Joo, H. Ko, An ice-templated, pH-tunable self-assembly route to hierarchically porous graphene nanoscroll networks. Nanoscale **6**, 9734 (2014)

24. P. Divya, S. Ramaprabhu, Hydrogen storage in platinum decorated hydrogen exfoliated graphene sheets by spillover mechanism. Phys. Chem. Chem. Phys. **16**, 26725 (2014)

25. L.J. Wang, J. Zhang, X. Zhao, L.L. Xu, Z.Y. Lyu, M. Lai, W. Chen, Palladium nanoparticle functionalized graphene nanosheets for Li–O2 batteries: enhanced performance by tailoring the morphology of the discharge product. RSC Adv. **5**, 73451 (2015)

26. H. Tao, X. Sun, S. Back, Z. Han, Q. Zhu, A.W. Robertson, T. Ma, Q. Fan, B. Han, Y. Jung, Doping palladium with tellurium for the highly selective electrocatalytic reduction of aqueous CO2 to CO. Chem. Sci. **9**, 483 (2018)

27. S.R. de Miguel, I.M.J. Vilella, P. Zgolicz, S.A. Bocanegra, Bimetallic catalysts supported on novel spherical MgAl2O4-coated supports for dehydrogenation processes. Appl. Catal. A **567**, 36 (2018)

28. M. Baca, K. Cendrowski, W. Kukulka, G. Bazarko, D. Moszyński, B. Michalkiewicz, R.J. Kalenczuk, B. Zielinska, A comparison of hydrogen storage in Pt, Pd and Pt/Pd alloys loaded disordered mesoporous hollow carbon spheres. Nanomaterials **8**, 639 (2018)

29. B.D. Adams, C.K. Ostrom, S. Chen, A. Chen, High-performance Pd-based hydrogen spillover catalysts for hydrogen storage. J. Phys. Chem. C **114**, 19875 (2010)

30. S.B. Singh, M. De, Thermally exfoliated graphene oxide for hydrogen storage. Mater. Chem. Phys. **239**, 122102 (2020)